Numerical Solutions of Induced Velocities by Semi-Infinite Tip Vortex Lines

Yihwan Danny Chiu* and David A. Peters†
Georgia Institute of Technology, Atlanta, Georgia

The method of Rand and Rosen[9] (for improving convergence on computed axial induced velocity for a helical wake) is extended to include all velocity components, all points in the wake, and nonhelical vortex lines (contraction). The method is based on finding upper and lower bounds on the truncated integral. Comparisons with other methods show that the present approach is efficient and accurate. Further, it avoids the errors associated with discretization of the vortex lines. Convergence occurs in only three to five revolutions, about 10% of the normal requirement.

Nomenclature

A	= wake constant in radial coordinate equation, Eq. (19b)
b	= number of blades
k_1, k_2	= parameters defining the average axial velocity of a tip-vortex element
R	= blade radius
r	$= (x_i^2 + y_i^2)^{1/2}/R$, radius of the control point
U_{ij}, V_{ij}, W_{ij}	= components of induced velocity at the control point i
V_0	= axial freestream velocity
v_i	= average induced velocity for undistorted wake model, or induced velocity at (x_0, y_0, z_0) at previous iteration for distorted and free-wake models
x_i, y_i, z_i	= coordinates of the control point
x_j, y_j, z_j	= coordinates of a segment of the trailing vortex line
x_0, y_0, z_0	= coordinates of the starting point of the trailing vortex line
x_j	$= \eta \cos(\theta + \theta_n)$
y_j	$= \eta \sin(\theta + \theta_n)$
z_i	$= \nu'(\theta - \delta) + z_0$
η	$= (x_0^2 + y_0^2)^{1/2}/R$, radius of the trailing vortex line
η'	$= d\eta/d\theta$, Eq. (19c)
θ	= angle of turning of the blade
θ'	$= \theta_n + \theta$
θ_n	$= 2\pi(n-1)/b$
δ	$= \tan^{-1}(y_0/x_0)$
ϕ	$= \tan^{-1}(y_i/x_i)$
λ	= wake constant in radial coordinate equation, Eq. (19b)
ν'	$= (V_0 + v_i)/R\omega$, inflow ratio
ω	= angular rotating velocity

Received Nov. 20, 1986; revision received June 12, 1987.
Copyright © American Institute of Aeronautics and Astronautics, Inc., 1987. All rights reserved.

*Research Assistant, School of Aerospace Engineering.
†Professor, School of Aerospace Engineering. Associate Fellow, AIAA

Introduction

In order to calculate the local aerodynamic behavior of rotating blades (such as aircraft propellers, marine propellers, helicopter rotors, etc.), application of lifting-surface theory is required. This is especially true when one studies the flow around the tips of blades with low aspect ratio, for which the classical approach of lifting-line theory is not applicable. Some researchers employ the vortex lattice method (VLM) that amounts to a Cauchy-type finite-element solution to lifting-surface problems. Many applications of VLM to problems of aerodynamic analysis and design of fixed wings have met with considerable success.[1-3] One reason for this success stems from the fact that the cost of computing the effect of the trailing vortex lines can be minimized (for the case of a wing) by use of efficient mathematical techniques. In the case of rotary wings, however, these fixed-wing techniques are not directly applicable. In the undistorted wake model, the calculation of induced velocities involves an integral with a semi-infinite limit for which no closed-form analytic solution exists as in the case of a fixed wing. Therefore, these integrals must be calculated numerically. Different researchers have developed various methods to improve the efficiency of this trailing vortex computation. Chang and Sullivan[4] terminate their calculations after 10 revolutions of the vortex helix. Baskin[5] carries out the numerical integration with an automatic selection of the upper limit, so that the absolute error of the obtained results does not exceed 10^{-4}. However, numerical results show that *several thousand* revolutions are required to obtain this accuracy. In the prescribed and free-wake models, the so-called "far wake" also causes difficulty in the calculation of induced velocities. Summa[6] and Hess[7] replace the vortex line by a semi-infinite cylindrical wake from infinitely many blades. Analytic solutions exist for the velocities induced by such a cylinder,[8] and this allows an efficient treatment.

Recently, a numerical technique has been developed by Rand and Rosen[9] to calculate the axial velocity induced by semi-infinite helical vortex lines. In Ref. 10, Rosen and Garber mention that they extended this method to calculate radial velocities as well; and, since the submission of our manuscript, the results of their effort have been documented in Ref. 11. The purpose of this paper is to extend their work to calculate all velocity components (including circumferential velocity) induced by semi-infinite helical lines. Further, this paper also extends the method to calculate all three velocity components induced by nonhelical vortex lines, pro-

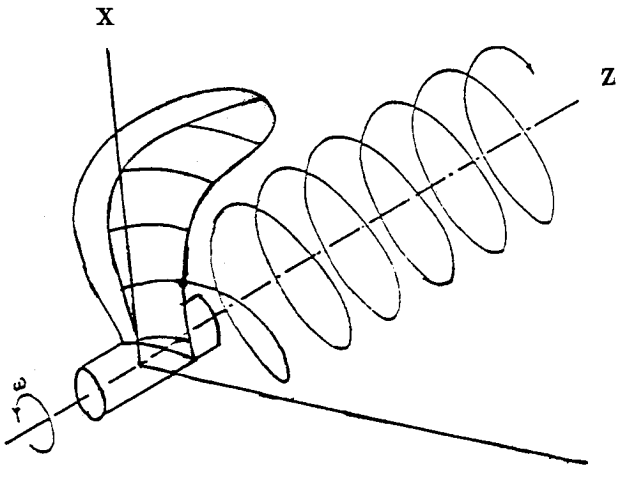

Fig. 1 Vortex coordinate system.

vided the trajectory of these lines is known as a function of azimuth. For example, the method can be applied to the case of wake contraction. It should be noted that the calculation of induced velocity is not limited to points along the blade. The methods described here apply to any point in the flowfield, the fact of which is also important in the panel method to account for the nonlifting portions.

Theoretical Derivation for Helical Vortex Lines

As shown in Fig. 1, an (x, y, z) Cartesian coordinate system originates from the center of the hub. The axis system is defined by taking an x axis through the trailing edge of the blade at the root, a z axis pointing to the positive downwind direction, and a y axis that completes the right-hand system. We define u_{ij}, v_{ij}, and w_{ij} as (x, y, z) components of induced velocity at a control point (x_i, y_i, z_i) and generated by a small helical vortex segment at the point (x_j, y_j, z_j) on the helical trailing vortex line that emanates form the point (x_0, y_0, z_0) with circulation equal to one. [The point $(x_0, y_0\ z_0)$ should lie on the trailing edge of the airfoil for the undistorted wake model or in the last point of the distorted vortex line in the near-wake region for the presecribed or free-wake model.] If we consider only the axial flight condition, the total normalized induced velocities induced by helical vortex lines (including those form other blades) U_{ij}, V_{ij}, W_{ij} can be determined by use of the Biot-Savart law:

$$U'_{ij}=\frac{1}{4\pi R}\,U_{ij}=\frac{1}{4\pi R}\int_0^\infty u_{ij}\mathrm{d}\theta \tag{1}$$

$$V'_{ij}=\frac{1}{4\pi R}\,V_{ij}=\frac{1}{4\pi R}\int_0^\infty v_{ij}\mathrm{d}\theta \tag{2}$$

$$W'_{ij}=\frac{1}{4\pi R}\,W_{ij}=\frac{1}{4\pi R}\int_0^\infty w_{ij}\mathrm{d}\theta \tag{3}$$

$$u_{ij}=\sum_{n=1}^{b}\frac{\nu'\{\eta\sin(\theta'+\delta)-r\sin(\phi)-[\theta+(z_0-z_i)/\nu']\eta\cos(\theta'+\delta)\}}{[\eta^2+r^2-2r\eta\cos(\theta'+\delta-\phi)+(\nu'\theta+z_0-z_i)^2]^{3/2}} \tag{4}$$

$$v_{ij}=\sum_{n=1}^{b}\frac{\nu'\{-\eta\cos(\theta'+\delta)+r\cos(\phi)-[\theta+(z_0-z_i)/\nu']\eta\sin(\theta'+\delta)\}}{[\eta^2+r^2-2r\eta\cos(\theta'+\delta-\phi)+(\nu'\theta+z_0-z_i)^2]^{3/2}} \tag{5}$$

$$w_{ij}=\sum_{n=1}^{b}\frac{\eta^2-r\eta\cos(\theta'+\delta-\phi)}{[\eta^2+r^2-2r\eta\cos(\theta'+\delta-\phi)+(\nu'\theta+z_0-z_i)^2]^{3/2}} \tag{6}$$

Table 1 Slope of error curve N for induced velocities

Velocity	N, uncorrected	N, corrected
U_{ij}	2	5
V_{ij}	2	5
*W_{ij}	2	6

*Note: W_{ij} is not truly an error, but is nearly so because $W_{ij}\approx 0$.

We note here that for $y_j=0$, (U_{ij}, V_{ij}, W_{ij}) are radial, circumferential, and axial components, respectively. The expressions for U_{ij}, V_{ij}, W_{ij} are very similar to those contained in other references. See for example, Ref. 4, Eqs. (2.8-2.11), or Ref. 5, Eq. (8.11).

The problem considered here is how to compute Eqs. (1), (2), and (3) which do not have closed-form analytic solutions. Reference 9 uses a combination of numerical and analytic solutions to calculate W_{ij}. According to this method, the numerical integration is carried only to a certain azimuth angle. Beyond this azimuth angle (to infinity), the integral is evaluated from the average of two analytic integrals that form the lower and upper bounds of the real integrand. The purpose of this paper is to discover if a similar approach can be developed for applications to both radial and circumferential velocities. Also, the crux of the matter lies in assessing how to find the lower and upper bounds of the real integrand for other cases.

A. Axial Induced Velocity (Along the z Axis Direction)

As described in Ref. 9, w_{ij} is usually bounded by the functions w_1 and w_2 that are defined as follows:

$$w_1=\sum_{n=1}^{b}\frac{\eta^2-r\eta\cos(\theta_n+\delta-\phi)}{\eta^2+r^2-2r\eta\cos(\theta_n+\delta-\phi)+(\nu'\theta+z_0-z_i)^2} \tag{7}$$

$$w_2=\sum_{n=1}^{b}\frac{\eta^2-r\eta\cos(\theta_n+\delta-\phi+\pi/b)}{\eta^2+r^2-2r\eta\cos(\theta_n+\delta-\phi+\pi/b)+(\nu'\theta+z_0-z_i)^2} \tag{8}$$

For sufficiently high values of θ, it is possible to assume that

$$w_{ij}\approx \tfrac{1}{2}(w_1+w_2) \tag{9}$$

Therefore, instead of Eq. (1), the following approximation may be used:

$$W_{ij}\approx\int_0^{\theta_m} w_{ij}\mathrm{d}\theta+\frac{1}{2}\left(\int_{\theta_m}^{\infty} w_1\mathrm{d}\theta+\int_{\theta_m}^{\infty} w_2\mathrm{d}\theta\right) \tag{10}$$

The main advantage of Eq. (10) is that the two integrals within the parentheses have closed-form analytic solutions as follows:

$$\int_{\theta_m}^{\infty} w_1 \mathrm{d}\theta = \sum_{n=1}^{b} \left[\frac{\eta^2 - r\eta \cos(\theta_n + \delta - \phi)}{[\eta^2 + r^2 - 2r\eta \cos(\theta_n + \delta - \phi)]\nu'} \times \left(1 - \frac{[\theta_m + (z_0 - z_i)/\nu']}{\{[\theta_m + (z_0 - z_i)/\nu']^2 + [\eta^2 + r^2 - 2r\eta \cos(\theta_n + \delta - \phi)]/(\nu')^2\}^{1/2}} \right) \right] \tag{11}$$

$$\int_{\theta_m}^{\infty} w_2 \mathrm{d}\theta = \sum_{n=1}^{b} \left[\frac{\eta^2 - r\eta \cos(\theta_n + \delta - \phi + \pi/b)}{[\eta^2 + r^2 - 2r\eta \cos(\theta_n + \delta - \phi + \pi/b)]\nu'} \times \left(1 - \frac{[\theta_m + (z_0 - z_i)/\nu']}{\{[\theta_m + (z_0 - z_i)/\nu']^2 + [\eta^2 + r^2 - 2r\eta \cos(\theta_n + \delta - \phi + \pi/b)]/(\nu')^2\}^{1/2}} \right) \right] \tag{12}$$

The foregoing result may be found in Ref. 9.

B. Radial Induced Velocity (Along the x Axis Direction)

We also find that the radial induced velocity u_{ij} is usually bounded by the functions u_1 and u_2 that are defined as follows:

$$u_1 = \sum_{n=1}^{b} \frac{\nu' \{\eta \sin(\theta_n + \delta) - r \sin(\phi) - [\theta + (z_0 - z_i)/\nu']\eta \cos(\theta_n + \delta)\}}{[\eta^2 + r^2 - 2r\eta \cos(\theta_n + \delta - \phi) + (\nu'\theta + z_0 - z_i)^2]^{3/2}}$$

$$u_2 = \sum_{n=1}^{b} \frac{\nu' \{\eta \sin(\theta_n + \delta + \pi/b) - r \sin(\phi) - [\theta + (z_0 - z_i)/\nu']\eta \cos(\theta_n + \delta + \pi/b)\}}{[\eta^2 + r^2 - 2r\eta \cos(\theta_n + \delta - \phi + \pi/b) + (\nu'\theta + z_0 - z_i)^2]^{3/2}}$$

Therefore, we can find U_{ij} in a similar manner as

$$U_{ij} \approx \int_0^{\theta_m} u_{ij} \mathrm{d}\theta + \frac{1}{2}\left(\int_{\theta_m}^{\infty} u_1 \mathrm{d}\theta + \int_{\theta_m}^{\infty} u_2 \mathrm{d}\theta \right) \tag{13}$$

where

$$\int_{\theta_m}^{\infty} u_1 \mathrm{d}\theta = \sum_{n=1}^{b} \left[\frac{\eta \sin(\theta_n + \delta) - r \sin(\phi)}{[\eta^2 + r^2 - 2r\eta \cos(\theta_n + \delta - \phi)]} \times \left(1 - \frac{[\theta_m + (z_0 - z_i)/\nu']}{\{[\theta_m + (z_0 - z_i)/\nu']^2 + [\eta^2 + r^2 - 2r\eta \cos(\theta_n + \delta - \phi)]/(\nu')^2\}^{1/2}} \right. \right.$$
$$\left. \left. - \frac{\eta \cos(\theta_n + \delta)}{(\nu')^2\{[\theta_m + (z_0 - z_i)/\nu']^2 + [\eta^2 + r^2 - 2r\eta \cos(\theta_n + \delta - \phi)]/(\nu')^2\}^{1/2}} \right] \tag{14}$$

$$\int_{\theta_m}^{\infty} u_2 \mathrm{d}\theta = \sum_{n=1}^{b} \left[\frac{\eta \sin(\theta_n + \delta + \pi/b) - r \sin(\phi)}{[\eta^2 + r^2 - 2r\eta \cos(\theta_n + \delta - \phi + \pi/b)]} \right.$$
$$\times \left(1 - \frac{[\theta_m + (z_0 - z_i)/\nu']}{\{[\theta_m + (z_0 - z_i)/\nu']^2 + [\eta^2 + r^2 - 2r\eta \cos(\theta_n + \delta - \phi + \pi/b)]/(\nu')^2\}^{1/2}} \right)$$
$$\left. - \frac{\eta \cos(\theta_n + \delta + \pi/b)}{(\nu')^2\{[\theta_m + (z_0 - z_i)/\nu']^2 + [\eta^2 + r^2 - 2r\eta \cos(\theta_n + \delta - \phi + \pi/b)]/(\nu')^2\}^{1/2}} \right] \tag{15}$$

This represents an original result, although the authors in Ref. 10 mention that they also have developed a similar formula. (That formula does indeed appear in Ref. 11, but it should be noted that the Cartesian components of the induced velocity are used here, whereas the approach in Ref. 11 is based on cylindrical coordinates.)

C. Circumferential Induced Velocity (Along the y Axis Direction)

Next, we find that the circumferential induced velocity V_{ij} is generally bounded by the functions v_1 and v_2 that are defined as follows:

$$v_1 = \sum_{n=1}^{b} \frac{\nu' \{-\eta \cos(\theta_n + \delta + \pi/2b) + r \cos(\phi) - [\theta + (z_0 - z_i)/\nu']\eta \cos(\theta_n + \delta + \pi/2b)\}}{[\eta^2 + r^2 - 2r\eta \cos(\theta_n + \delta - \phi + \pi/2b) + (\nu'\theta + z_0 - z_i)^2]^{3/2}}$$

$$v_2 = \sum_{n=1}^{b} \frac{\nu' \{-\eta \cos(\theta_n + \delta + 3\pi/2b) + r \cos(\phi) - [\theta + (z_0 - z_i)/\nu']\eta \cos(\theta_n + \delta + 3\pi/2b)\}}{[\eta^2 + r^2 - 2r\eta \cos(\theta_n + \delta - \phi + 3\pi/2b) + (\nu'\theta + z_0 - z_i)^2]^{3/2}}$$

Therefore, we can find V_{ij} in a similar manner as

$$V_{ij} \approx \int_0^{\theta_m} v_{ij} \mathrm{d}\theta + \frac{1}{2}\left(\int_{\theta_m}^{\infty} v_1 \mathrm{d}\theta + \int_{\theta_m}^{\infty} v_2 \mathrm{d}\theta \right) \tag{16}$$

where

$$\int_{\theta_m}^{\infty} v_1 d\theta = \sum_{n=1}^{b} \left[\frac{-\eta \cos(\theta_n+\delta+\pi/2b)+r\cos(\phi)}{[\eta^2+r^2-2r\eta\cos(\theta_n+\delta-\phi+\pi/2b)]} \times \left(1-\frac{[\theta_m+(z_0-z_i)/\nu']}{\{[\theta_m+(z_0-z_i)/\nu']^2+[\eta^2+r^2-2r\eta\cos(\theta_n+\delta-\phi+\pi/2b)]/(\nu')^2\}^{1/2}}\right) - \frac{\eta\sin(\theta_n+\delta+\pi/2b)}{(\nu')^2\{[\theta_m+(z_0-z_i)/\nu']^2+[\eta^2+r^2-2r\eta\cos(\theta_n+\delta-\phi+\pi/2b)]/(\nu')^2\}^{1/2}}\right] \tag{17}$$

$$\int_{\theta_m}^{\infty} v_2 d\theta = \sum_{n=1}^{b} \left[\frac{-\eta \cos(\theta_n+\delta+3\pi/2b)+r\cos(\phi)}{[\eta^2+r^2-2r\eta\cos(\theta_n+\delta-\phi+3\pi/2b)]} \times \left(1-\frac{[\theta_m+(z_0-z_i)/\nu']}{\{[\theta_m+(z_0-z_i)/\nu']^2+[\eta^2+r^2-2r\eta\cos(\theta_n+\delta-\phi+3\pi/2b)]/(\nu')^2\}^{1/2}}\right) - \frac{\eta\sin(\theta_n+\delta+3\pi/2b)}{(\nu')^2\{[\theta_m+(z_0-z_i)/\nu']^2+[\eta^2+r^2-2r\eta\cos(\theta_n+\delta-\phi+3\pi/2b)]/(\nu')^2\}^{1/2}}\right] \tag{18}$$

The aforementioned are also the original results of our work.

Theoretical Derivation with Wake Contraction

In this section, we extend the technique proposed to the calculation of velocities induced by contracting vortex lines. In helicopter work, it is known that wake contraction has a significant effect on the induced flow at the rotor disk. The detailed trajectory of prescribed tip vortex lines (i.e., the wake coordinates) is available in the hovering case. Two options[12-13] for high aspect ratio blades are verified by Tung[14] and Norman[15] as follows: 1) the Kocurek[12] wake and 2) the Landgrebe[13] wake. In general, the wake coordinates derived from Refs. 12 and 13 should be shifted by a transformation matrix according to the coning and offset-hinge coupling effects to determine the relative position of the wake to the blades. However, in order to simplify this problem, we consider only the case for which the coning and offset-hinge coupling effects are negligible and for which the tip vortex lines emanate from the trailing edge of airfoil, assumed to lie on the x axis. Then, $y_0 = z_0 = \delta = 0$ holds true for this simplified assumption. Also, only the Landgrebe wake is considered here.

As described in Ref. 13, the tip vortex from a single blade is approximated by the following geometric relations:

$$z_j = \begin{cases} k_1\theta & \text{for } 0 \le \theta \le 2\pi/b \\ (z_j)_{\theta=2\pi/b} + k_2(\theta - 2\pi/b) & \text{for } \theta \ge 2\pi/b \end{cases} \tag{19a}$$

$$\eta = A + (1-A)e^{-\lambda\theta} \tag{19b}$$

$$\eta' = \lambda(A-1)e^{-\lambda\theta} \tag{19c}$$

The four parameters (k_1, k_2, A, λ) are determined either from experimental tests or taken as known functions of thrust coefficient and blade geometry.[13] The major difference between contracted tip-vortex lines and noncontracted, helical vortex lines is that η is not a constant in the former case. Equations (1-3) are still valid if we define u_{ij}, v_{ij}, w_{ij} as follows:

For $\theta \le 2\pi/b$

$$u_{ij} = \sum_{n=1}^{b} \frac{k_1\{\eta\sin(\theta') - r\sin(\phi) - (\theta - z_i/k_1)[\eta\cos(\theta')+\eta'\sin(\theta')]\}}{[\eta^2+r^2-2r\eta\cos(\theta'-\phi)+(k_1\theta-z_i)^2]^{3/2}}$$

$$v_{ij} = \sum_{n=1}^{b} \frac{k_1\{-\eta\cos(\theta') + r\cos(\phi) - (\theta - z_i/k_1)[\eta\sin(\theta')-\eta'\cos(\theta')]\}}{[\eta^2+r^2-2r\eta\cos(\theta'-\phi)+(k_1\theta-z_i)^2]^{3/2}}$$

$$w_{ij} = \sum_{n=1}^{b} \frac{\eta^2 - r\eta\cos(\theta'-\phi) - \eta' r\sin(\theta'-\phi)}{[\eta^2+r^2-2r\eta\cos(\theta'-\phi)+(k_1\theta-z_i)^2]^{3/2}}$$

For $\theta \ge 2\pi/b$

$$u_{ij} = \sum_{n=1}^{b} \frac{k_2\{\eta\sin(\theta') - r\sin(\phi) - [(k_1/k_2-1)2\pi/b + \theta - z_i/k_2][\eta\cos(\theta')+\eta'\sin(\theta')]\}}{[\eta^2+r^2-2r\eta\cos(\theta'-\phi)+(z_j-z_i)^2]^{3/2}}$$

$$v_{ij} = \sum_{n=1}^{b} \frac{k_2\{-\eta\cos(\theta') + r\cos(\phi) - [(k_1/k_2-1)2\pi/b + \theta - z_i/k_2][\eta\sin(\theta')-\eta'\cos(\theta')]\}}{[\eta^2+r^2-2r\eta\cos(\theta'-\phi)+(z_j-z_i)^2]^{3/2}}$$

$$w_{ij} = \sum_{n=1}^{b} \frac{\eta^2 - r\eta\cos(\theta'-\phi) - \eta' r\sin(\theta'-\phi)}{[\eta^2+r^2-2r\eta\cos(\theta'-\phi)+(z_j-z_i)^2]^{3/2}}$$

Inspection of the above equations suggests corresponding formulas for the upper and lower bounds of (U_{ij}, V_{ij}, W_{ij}) including wake contraction. These functions are also constructed so as to have closed-form integrals where

$$w_1 = \sum_{n=1}^{b} \frac{\eta^2 - r\eta\cos(\theta_n - \phi) - \eta' r \sin(\theta_n - \phi)}{\eta^2 + r^2 - 2r\eta\cos(\theta_n - \phi) + (z_j - z_i)^2}$$

$$w_2 = \sum_{n=1}^{b} \frac{\eta^2 - r\eta\cos(\theta_n - \phi + \pi/b) - \eta' r \sin(\theta_n - \phi + \pi/b)}{\eta^2 + r^2 - 2r\eta\cos(\theta_n - \phi + \pi/b) + (z_j - z_i)^2}$$

$$\int_{\theta_m}^{\infty} w_1 d\theta = \sum_{n=1}^{b} \left[\frac{\eta^2 - r\eta\cos(\theta_n - \phi) - \eta' r \sin(\theta_n - \phi)}{[\eta^2 + r^2 - 2r\eta\cos(\theta_n - \phi)]k_2} \times \left(1 - \frac{[\theta_m + (k_1/k_2 - 1)2\pi/b - z_i/k_2]}{\{[\theta_m + (k_1/k_2 - 1)2\pi/b - z_i/k_2]^2 + [\eta^2 + r^2 - 2r\eta\cos(\theta_n - \phi)]/(k_2)^2\}^{1/2}}\right)\right] \tag{20}$$

$$\int_{\theta_m}^{\infty} w_2 d\theta = \sum_{n=1}^{b} \left[\frac{\eta^2 - r\eta\cos(\theta_n - \phi + \pi/b) - \eta' r \sin(\theta_n - \phi + \pi/b)}{[\eta^2 + r^2 - 2r\eta\cos(\theta_n - \phi + \pi/b)]k_2} \times \left(1 - \frac{[\theta_m + (k_1/k_2 - 1)2\pi/b - z_i/k_2]}{\{[\theta_m + (k_1/k_2 - 1)2\pi/b - z_i/k_2]^2 + [\eta^2 + r^2 - 2r\eta\cos(\theta_n - \phi + \pi/b)]/(k_2)^2\}^{1/2}}\right)\right] \tag{21}$$

$$u_1 = \sum_{n=1}^{b} \frac{k_2\{\eta \sin(\theta_n) - r\sin(\phi) - [(z_j - z_i)/k_2][\eta\cos(\theta_n) + \eta' \sin(\theta_n)]\}}{[\eta^2 + r^2 - 2r\eta\cos(\theta_n - \phi) + (z_j - z_i)^2]^{3/2}}$$

$$u_2 = \sum_{n=1}^{b} \frac{k_2\{\eta \sin(\theta_n + \pi/b) - r\sin(\phi) - [(z_j - z_i)/k_2][\eta\cos(\theta_n + \pi/b) + \eta' \sin(\theta_n + \pi/b)]\}}{[\eta^2 + r^2 - 2r\eta\cos(\theta_n - \phi + \pi/b) + (z_j - z_i)^2]^{3/2}}$$

$$\int_{\theta_m}^{\infty} u_1 d\theta = \sum_{n=1}^{b} \left[\frac{\eta\sin(\theta_n) - r\sin(\phi)}{[\eta^2 + r^2 - 2r\eta\cos(\theta_n - \phi)]} \times \left(1 - \frac{[\theta_m + (k_1/k_2 - 1)2\pi/b - z_i/k_2]}{\{[\theta_m + (k_1/k_2 - 1)2\pi/b - z_i/k_2]^2 + [\eta^2 + r^2 - 2r\eta\cos(\theta_n - \phi)]/(k_2)^2\}^{1/2}}\right) - \frac{\eta\cos(\theta_n) + \eta' \sin(\theta_n)}{(k_2)^2\{[\theta_m + (k_1/k_2 - 1)2\pi/b - z_i/k_2]^2 + [\eta^2 + r^2 - 2r\eta\cos(\theta_n - \phi)]/(k_2)^2\}^{1/2}}\right] \tag{22}$$

$$\int_{\theta_m}^{\infty} u_2 d\theta = \sum_{n=1}^{b} \left[\frac{\eta\sin(\theta_n + \pi/b) - r\sin(\phi)}{[\eta^2 + r^2 - 2r\eta\cos(\theta_n - \phi + \pi/b)]} \times \left(1 - \frac{[\theta_m + (k_1/k_2 - 1)2\pi/b - z_i/k_2]}{\{[\theta_m + (k_1/k_2 - 1)2\pi/b - z_i/k_2]^2 + [\eta^2 + r^2 - 2r\eta\cos(\theta_n - \phi + \pi/b)]/(k_2)^2\}^{1/2}}\right) - \frac{\eta\cos(\theta_n + \pi/b) + \eta' \sin(\theta_n + \pi/b)}{(k_2)^2\{[\theta_m + (k_1/k_2 - 1)2\pi/b - z_i/k_2]^2 + [\eta^2 + r^2 - 2r\eta\cos(\theta_n - \phi + \pi/b)]/(k_2)^2\}^{1/2}}\right] \tag{23}$$

$$v_1 = \sum_{n=1}^{b} \frac{k_2\{-\eta\cos(\theta_n + \pi/2b) + r\cos(\phi) - [(z_j - z_i)/k_2][\eta\sin(\theta_n + (\pi/2b) - \eta' \cos(\theta_n + \pi/2b)]\}}{\{\eta^2 + r^2 - 2r\eta\cos(\theta_n - \phi + \pi/2b) + (z_j - z_i)^2]^{3/2}}$$

$$v_2 = \sum_{n=1}^{b} \frac{k_2\{-\eta\cos(\theta_n + 3\pi/2b) + r\cos(\phi) - [(z_j - z_i)/k_2][\eta\sin(\theta_n + 3\pi/2b) - \eta' \cos(\theta_n + 3\pi/2b)]\}}{[\eta^2 + r^2 - 2r\eta\cos(\theta_n - \phi + 3\pi/2b) + (z_k - z_i)^2]^{3/2}}$$

$$\int_{\theta_m}^{\infty} v_1 d\theta = \sum_{n=1}^{b} \left[\frac{-\eta\cos(\theta_n + \pi/2b) + r\cos(\phi)}{[\eta^2 + r^2 - 2r\eta\cos(\theta_n - \phi + \pi/2b)]} \times \left(1 - \frac{[\theta_m + (k_1/k_2 - 1)2\pi/b - z_i/k_2]}{\{[\theta_m + (k_1/k_2 - 1)2\pi/b - z_i/k_2]^2 + [\eta^2 + r^2 - 2r\eta\cos(\theta_n - \phi + \pi/2b)]/(k_2)^2\}^{1/2}}\right) - \frac{\eta\sin(\theta_n + \pi/2b) - \eta' \cos(\theta_n + (\pi/2b)}{(k_2)^2\{[\theta_m + (k_1/k_2 - 1)2\pi/b - z_i/k_2]^2 + [\eta^2 + r^2 - 2r\eta\cos(\theta_n - \phi + (\pi/2b)]/(k_2)^2\}^{1/2}}\right] \tag{24}$$

$$\int_{\theta_m}^{\infty} v_2 d\theta = \sum_{n=1}^{b} \left[\frac{-\eta \cos(\theta_n + 3\pi/2b) + r\cos(\phi)}{[\eta^2 + r^2 - 2r\eta \cos(\theta_n - \phi + 3\pi/2b)]} \right.$$
$$\times \left(1 - \frac{[\theta_m + (k_1/k_2 - 1)2\pi/b - z_i/k_2]}{\{[\theta_m + (k_1/k_2 - 1)2\pi/b - z_i/k_2]^2 + [\eta^2 + r^2 - 2r\eta \cos(\theta_n - \phi + 3\pi/2b)]/(k_2)^2\}^{1/2}}\right)$$
$$\left. - \frac{\eta \sin(\theta_n + 3\pi/2b) - \eta' \cos(\theta_n + 3\pi/2b)}{(k_2)^2\{[\theta_m + (k_1/k_2 - 1)2\pi/b - z_i/k_2]^2 + [\eta^2 + r^2 - 2r\eta \cos(\theta_n - \phi + 3\pi/2b)]/(k_2)^2\}^{1/2}} \right] \quad (25)$$

With these formulas, the induced velocities may be estimated as per Eqs. (10), (13), and (16). Several things should be noted: 1) θ_m should be greater than $b/2\pi$, 2) tip vortex lines from other blades are included, 3) η and η' are functions of θ, and 4) the strength of the vortex is assumed to be unity. Also, if we consider the cases for which z_0 or δ is not equal to zero, Eqs. (20-25) still hold true by the following substitutions:

$$z_i \rightarrow z_i - z_0$$
$$\theta' \rightarrow \theta' + \delta$$
$$\theta_n \rightarrow \theta_n + \delta$$

Numerical Results

It is clear that, in general, the approximations of Eqs. (10), (13), and (16) improve as θ_m is increased. It is also clear that the accuracy of the approximation will be a function of ν', b, (x_i, y_i, z_i), and (x_0, y_0, z_0). Numerical results show that if we select θ_m around 30 to 40π, the absolute error of the integral will not exceed 10^{-4} for the undistorted wake model. A large value of $(z_0 - z_i)/\nu'$ has the same effect for the distorted and free-wake models as does an increase in θ_m for the helical wake. Therefore, an adequate θ_m should be slightly less than 30π. Also, the accuracy is sensitive to the location of θ_m. The error as a function of θ_m oscillates about some average value for either the corrected or uncorrected methods. By selecting either $\theta_m = \delta - \phi + m\pi$ (where m is an integer) for U_{ij}, W_{ij}, or $\theta_m = \delta - \phi + m\pi + \pi/(2b)$ for V_{ij}, we obtain values that are near this average for either case.

Figure 2 gives numerical results for the axial velocity W_{ij} at $x_i/R = 0.9$ (on the rotor blade) due to two vortices (i.e., a two-bladed rotor) emanating from $x_0/R = \pm 0.6$. The velocity is plotted as a function of θ_m, the maximum θ used in the integration. The circles are the values of the integral, Eq. (3), taken from 0 to θ_m; and the squares are the values of the integral obtained by the addition of the closed-form trailing terms to this result. This figure is, basically, a reproduction of the results in Ref. 9. Several points are noteworthy. First, although the "approximation" is derived from approximate closed-form results, it should give the exact answer as $\theta_m \rightarrow \infty$. The value of the exact answer is -1.9×10^{-4}. (One can show that this velocity should be zero for the case of an infinite number of blades because $v_0 < x_i$. As a consequence,

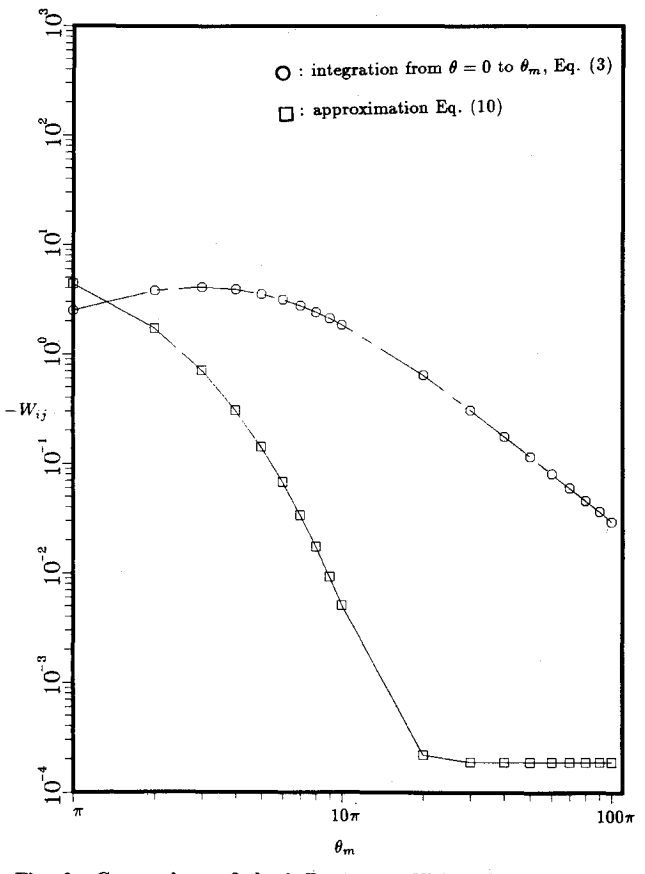

Fig. 2 Comparison of the influence coefficient W_{ij} as a function of the integration distance, θ_m, from Eqs. (3) and (10) [$b = 2$; $\nu' = 0.05$; $(x_i, y_i, z_i)/R = (0.9, 0, 0)$; $(z_0, y_0, z_0)/R = (0.6, 0, 0)$; exact value = -0.00019].

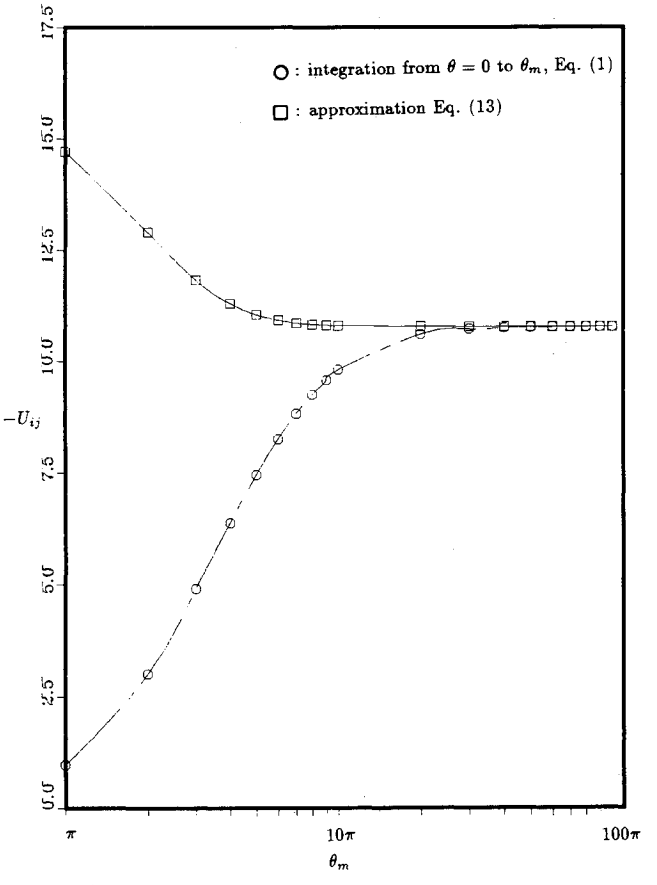

Fig. 3 Comparison of the influence coefficient U_{ij} as a function of the integration distance, θ_m, from Eqs. (1) and (13) [$b = 2$; $\nu' = 0.05$; $(x_i, y_i, z_i)/R = (0.9, 0, 0)$; $(z_0, y_0, z_0)/R = (0.6, 0, 0)$; exact value = -10.78459].

the value of W_{ij} is very small even for two blades.) To obtain a similar accuracy level without the trailing corrections would require integration over 500 revolutions of the helix. At $\theta_m = 10\pi$ (five revolutions of numerical integration), the error of the numerical integral is 2.0; but with the closed-form corrections, the error is only 0.005. Another way of viewing the results is that for a certian error (e.g., $W_{ij} = 0.01$), the old way requires 25 revolutions, whereas the corrected method requires only three revolutions.

Figures 3 and 4 give similar results for the radial induced velocity U_{ij} at the same point. Figure 3 illustrates the rapid convergence (with the closed-form correction) to the correct value of -10.8634. Figure 4, which gives percent error, illustrates in detail how much faster the convergence is. For example, 1% error requires 10 revolutions without the correction and only three revolutions with the correction (a similar trend to W_{ij}). Figures 5 and 6 complete the velocity set with circumferential induced velocity V_{ij}. Figure 5 shows the convergence of total velocity.

Figure 6 indicates that, for a 1% error, we require 25 revolutions without the correction and only three revolutions with the correction. The sharp spike in the curve is an indication of an antinode (a place for which the approximate curve crosses the exact value, giving a temporary zero in error). The upper envelope of points, however, is the true convergence.

It is also interesting to compare rates of convergence (i.e., slopes) in Figs. 2, 4, and 6. Table 1 gives the exponent N from error proportional to $(\theta_m)^{-N}$ for each case. Thus, the crorected formulas give over twice the rate of convergence of the direct integrals.

In the previous figures, we have looked at the velocity on the blade. Now, we turn to the velocity at 0.5 radii above the

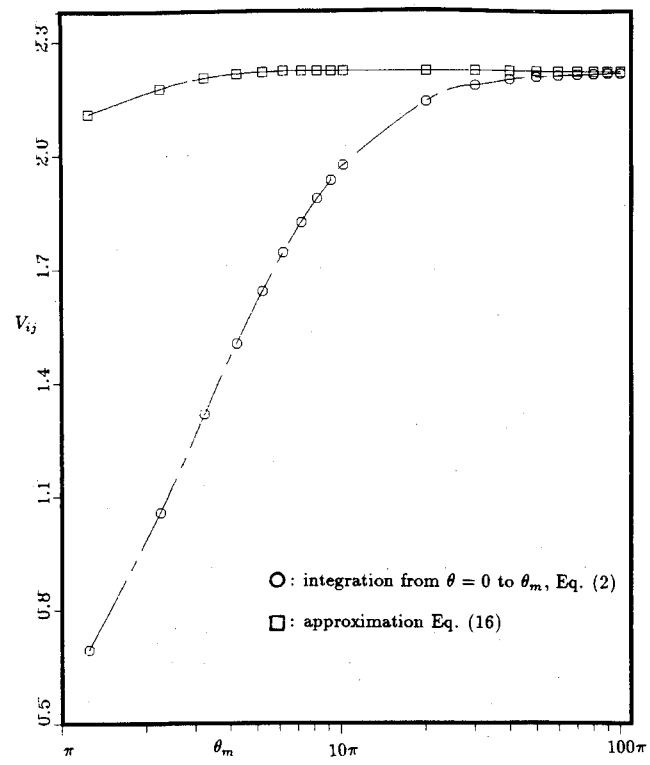

Fig. 5 Comparison of the influence coefficient V_{ij} as a function of the integration distance, θ_m, from Eqs. (2) and (16) [$b = 2$; $\nu' = 0.05$; $(x_i, y_i, z_i)/R = (0.9, 0, 0)$; $(z_0, y_0, z_0)/R = (0.6, 0, 0)$; exact value = 2.22223].

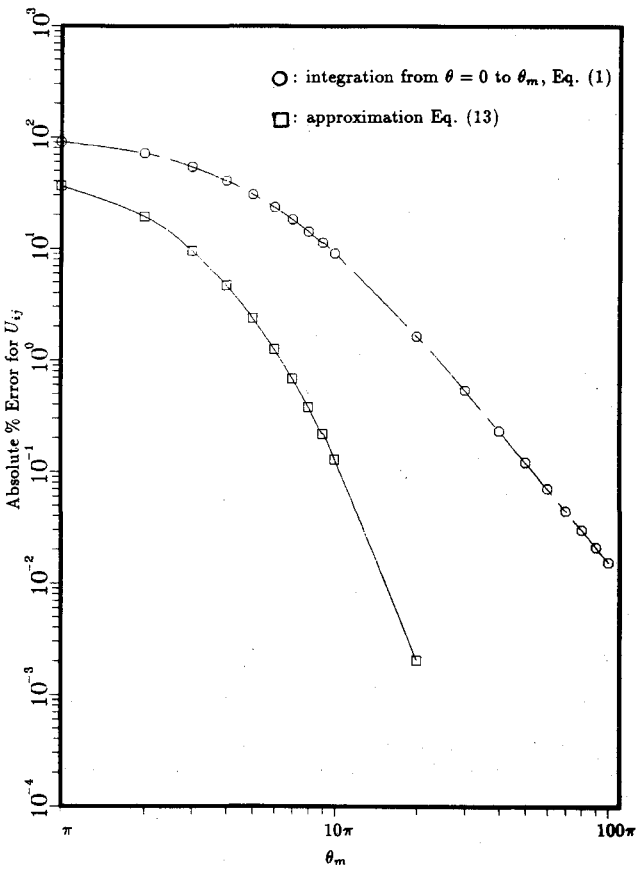

Fig. 4 Comparison of the percent error in U_{ij} as a function of the integration distance, θ_m, from Eqs. (1) and (13) [$b = 2$; $\nu' = 0.05$; $(x_i, y_i, z_i)/R = (0.9, 0, 0)$; $(z_0, y_0, z_0)/R = (0.6, 0, 0)$; exact value = -10.78459].

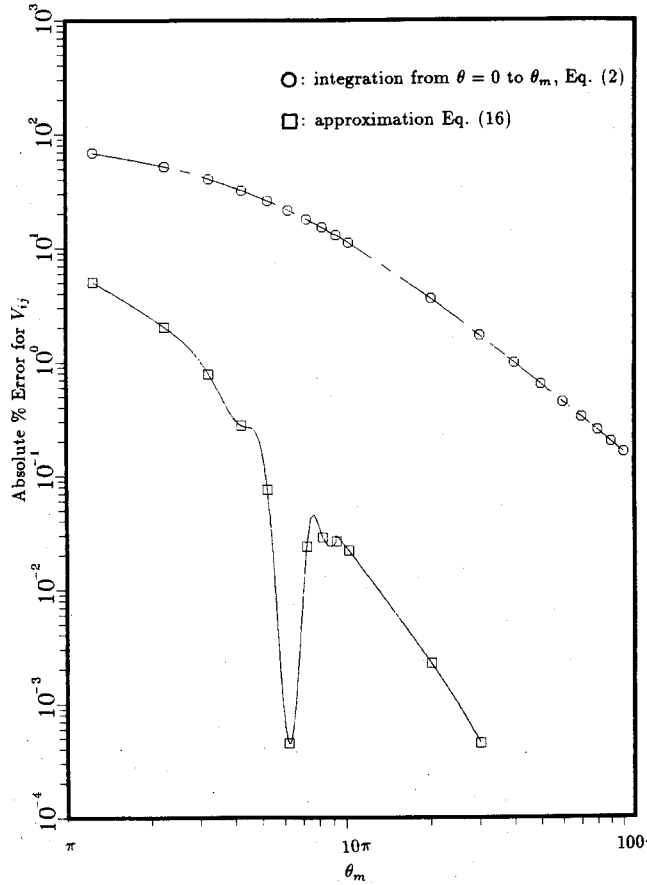

Fig. 6 Comparison of the percent error in V_{ij} as a function of the integration distance, θ_m, from Eqs. (2) and (16) [$b = 2$; $\nu' = 0.05$; $(x_i, y_i, z_i)/R = (0.9, 0, 0)$; $(z_0, y_0, z_0)/R = (0.6, 0, 0)$; exact value = 2.22223].

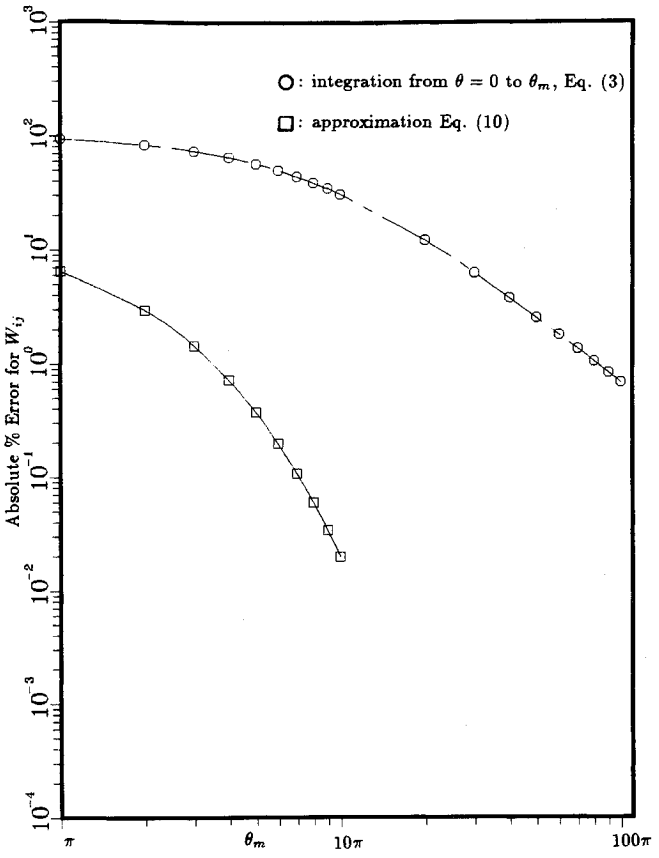

Fig. 7 Comparison of the influence coefficient W_{ij} as a function of the integration distance, θ_m, from Eqs. (3) and (10) [$b=2$; $\nu'=0.05$; $(x_i, y_i, z_i)/R=(0.9, 0, 0)$; $(z_0, y_0, z_0)/R=(0.6, 0, 0.5)$; exact value = 4.05635].

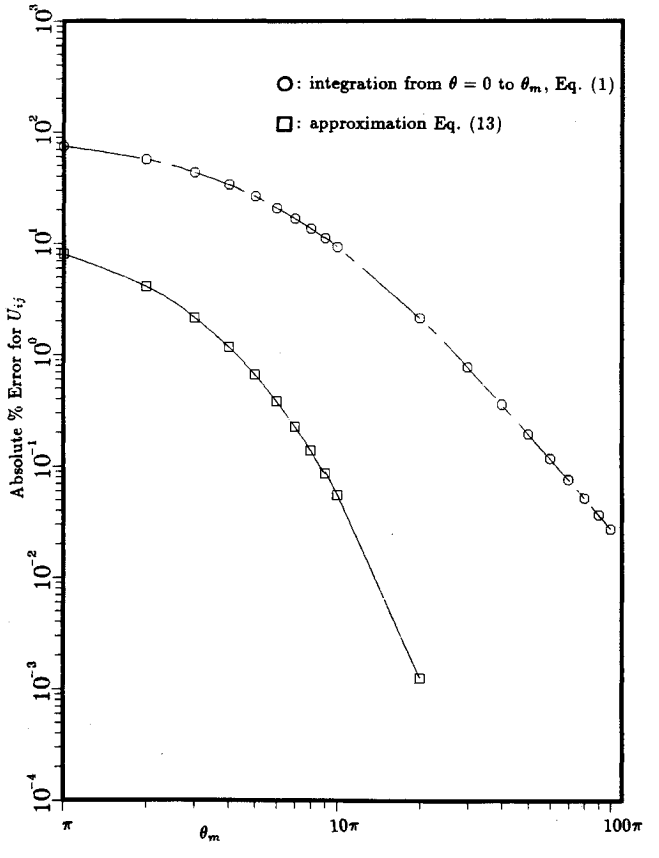

Fig. 8 Comparison of the influence coefficient U_{ij} as a function of the integration distance, θ_m, from Eqs. (1) and (13) [$b=2$; $\nu'=0.05$; $(x_i, y_i, z_i)/R=(0.9, 0, 0)$; $(z_0, y_0, z_0)/R=(0.6, 0, 0.5)$; exact value = −5.58698].

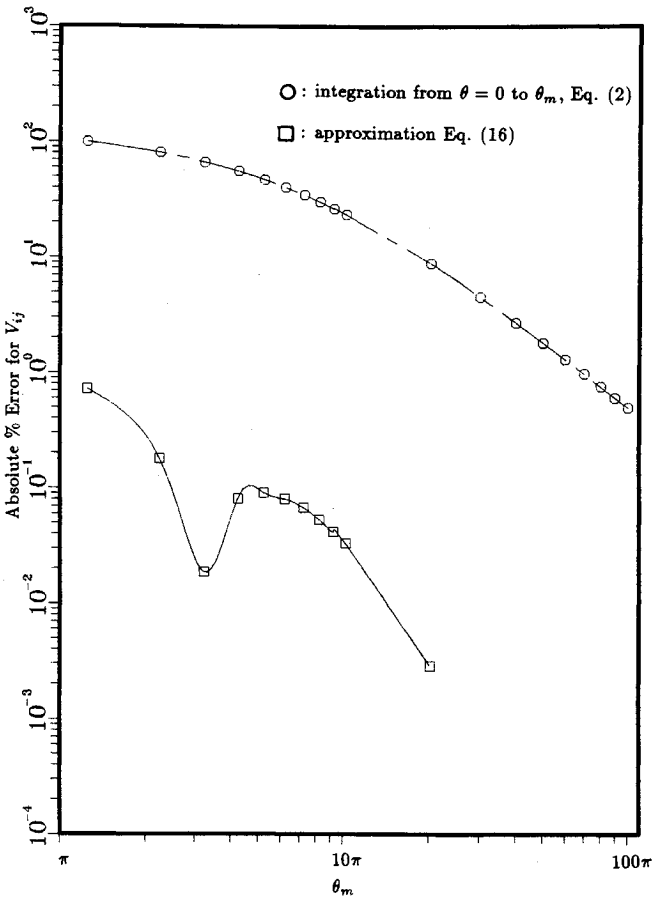

Fig. 9 Comparison of the influence coefficient V_{ij} as a function of the integration distance, θ_m, from Eqs. (2) and (16) [$b=2$; $\nu'=0.05$; $(x_i, y_i, z_i)/R=(0.9, 0, 0)$; $(z_0, y_0, z_0)/R=(0.6, 0, 0.5)$; exact value = 0.69274].

blade, $z_0/R=0.5$ (which is equivalent to $z_0/R=0$, $z_i/R=-0.5$). Figure 7 shows the result for the axial induced velocity W_{ij}. The rate of convergence is slow without the correction, and 40 revolutions will give 1% error. However, with the correction, only two revolutions can give the same accuracy. Figures 8 and 9 present the results for radial and circumferential velocities at the same point. These results have the same trend of convergence as those of control points on the blades. If z_i is less than z_0 (i.e, the control is above the helical lines), numerical results confirm that the rate of convergence with the correction is always faster than that without the correction.

In order to check these formulas for control points below the rotor plane, we also look at the velocity at 0.5 radius below the blade, $z_0/R=-0.5$ (which is equivalent to $z_0/R=0$, $z_i/R=0.5$). Figure 10 shows the result for the axial induced velocity W_{ij}. There is a small region, over the first two revolutions, for which the "uncorrected" curve is better than the corrected curve due to an error cross-over. However, after θ_m passes through the first few revolutions, the corrected curve exhibits the typical rapid convergence. Figure 10 reveals that, for 1% error, we require 45 revolutions without the correction but only five revolutions with the correction.

Figure 11 gives the results for the radial velocity U_{ij}. Both corrected and uncorrected curves have a hump over the first few revolutions. The rate of convergence with the correction is faster than that without the correction. For example, for 1% error we require 15 revolutions without the correction and only five revolutions with the correction. Figure 12 shows the result for the circumferential velocity V_{ij}. Here, the rate of convergence with the correction is still faster than that without the correction. Also, for 1% error, we require

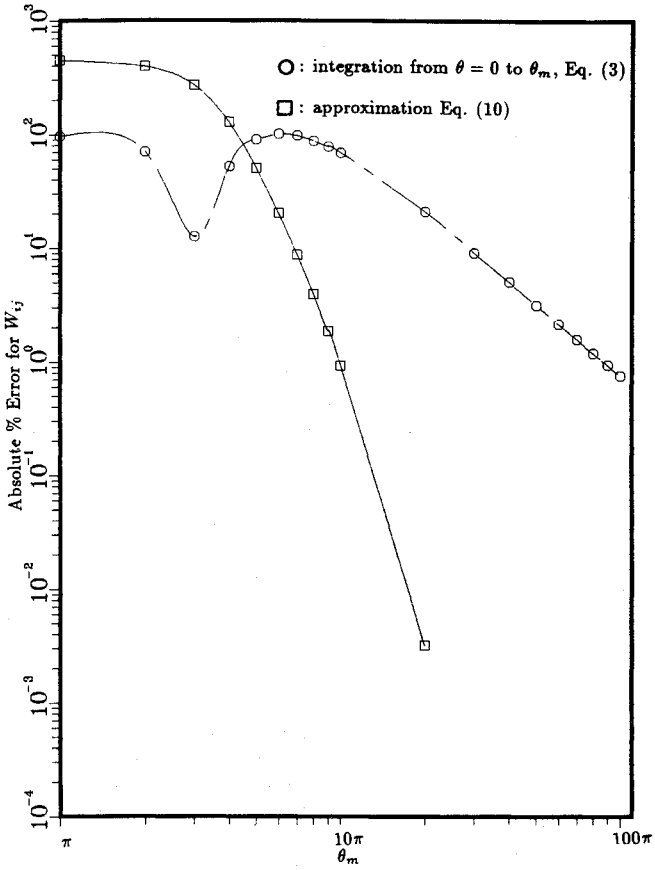

Fig. 10 Comparison of the influence coefficient W_{ij} as a function of the integration distance, θ_m, from Eqs. (3) and (10) [$b=2$; $\nu'=0.05$; $(x_i, y_i, z_i)/R=(0.9, 0, 0)$; $(z_0, y_0, z_0)/R=(0.6, 0, -0.5)$; exact value $=-4.05651$].

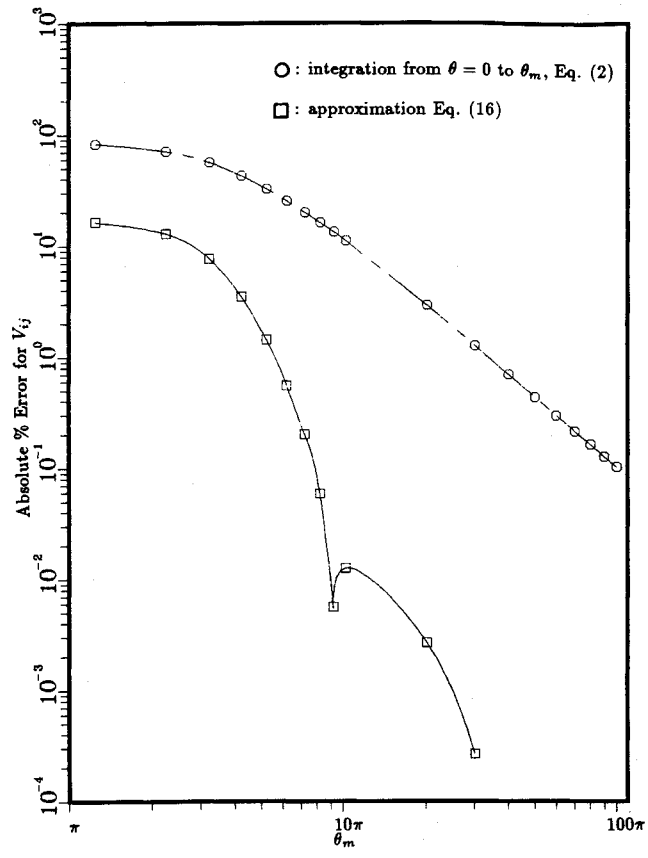

Fig. 12 Comparison of the influence coefficient V_{ij} as a function of the integration distance, θ_m, from Eqs. (2) and (16) [$b=2$; $\nu'=0.05$; $(x_i, y_i, z_i)/R=(0.9, 0, 0)$; $(z_0, y_0, z_0)/R=(0.6, 0, -5.0)$; exact value $=3.751733$].

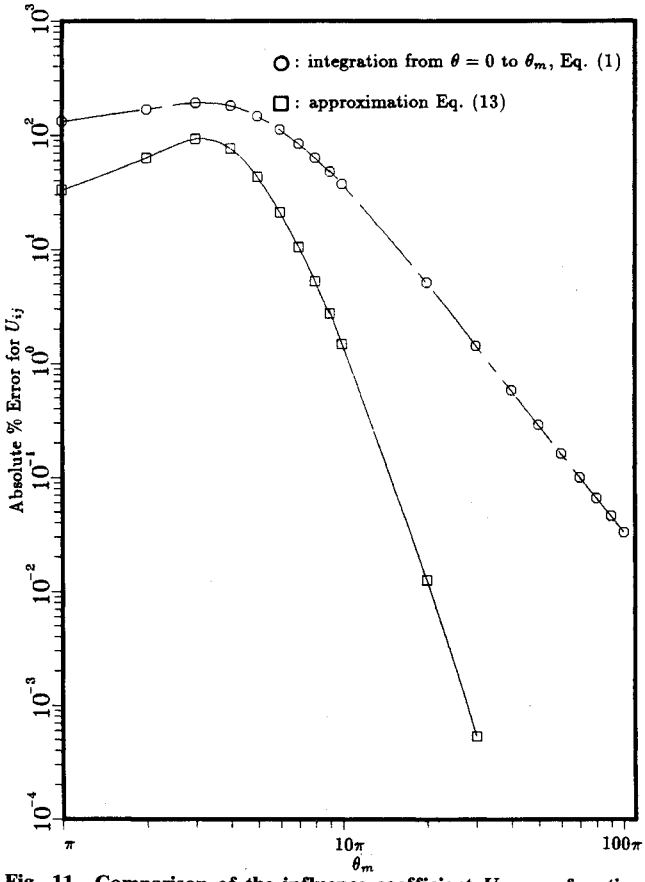

Fig. 11 Comparison of the influence coefficient U_{ij} as a function of the integration distance, θ_m, from Eqs. (1) and (13) [$b=2$; $\nu'=0.05$; $(x_i, y_i, z_i)/R=(0.9, 0, 0)$; $(z_0, y_0, z_0)/R=(0.6, 0, -0.5)$; exact value $=-5.58662$].

15 revolutions without the correction and only three revolutions with the correction.

We now turn to numerical results with wake contraction. In the most common methods of analyses for this case, investigators use straight[13] or curved[6] vortex segments in order to descretize the computation. Normal lenghts of these segments correspond to azimuthal steps ranging from $\Delta\theta=5$ deg to $\Delta\theta=15$ deg. Thus, there are two sources of error in such calculations. One is the truncation error, which results from truncation of the wake at some θ_m (as in the helical wake), and the other is the quadrature error that results form the descretization process (which is an approximation of the integral of vorticity). Very little work has been done on the effect of the quadrature error. In the method described in this paper, the vortex system is not broken into discrete filaments. Therefore, the error from the numerical integration is usually very small (normally 10^{-7} to 10^{-15}); and the truncation error dominates, although we try to minimize this truncation error by use of the closed-form correction. For conventional methods, however, both errors can be significant. Figure 13 illustrates these points. In this figure, the axial velocity W_{ij} is given at $x_i/R=0.95$ (on the blade) due to two contracted tip-vortex lines with $k_1=0.175$, $k_2=0.0424$, $A=0.78$, and $\lambda=0.1936$ (from experimental data[13]).

First, let us compare numerical integration (0 to θ_m) with the method of straight vortex segments. Since both have the same truncation error, this will reveal the qudrature error. Vortex-segment results are given for both $\Delta\theta=5$ deg and $\Delta\theta=15$ deg. In the range from π to 10π (0–5 revolutions), we see that the quadrature error is the opposite sign of the truncation error and actually *decreases* the total error. Therefore, the 15-deg segments (with more quadrature error) actually have less *total* error than do 5-deg segments. As θ_m in-

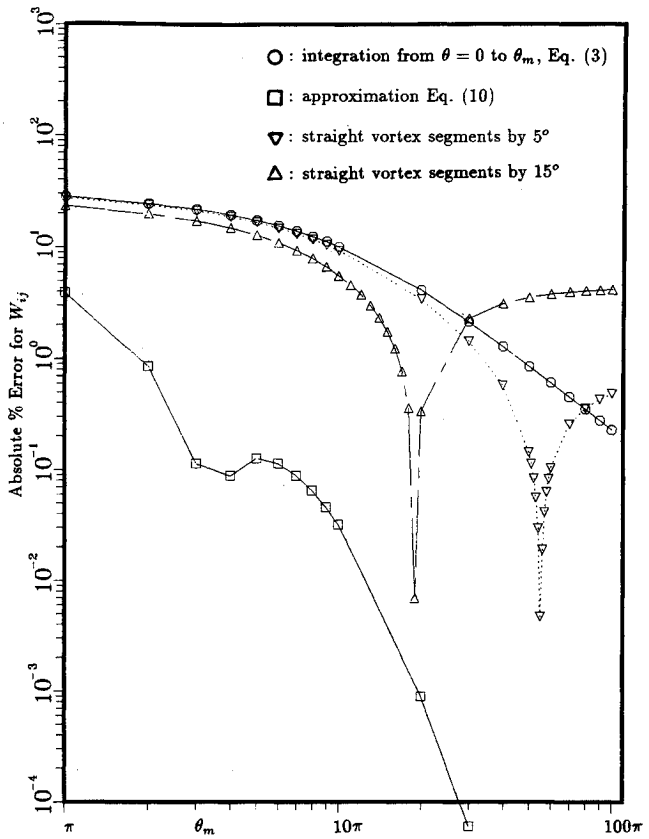

Fig. 13 Comparison of the influence coefficient W_{ij} with wake contraction as a function of the integration distance, θ_m, from Eqs. (3) and (10) [$b=2$; $k_1=0.125$; $k_2=0.0424$; $A=0.78$; $\lambda=0.1936$; $(x_i, y_i, z_i)/R=(0.95, 0, 0)$; exact value$=33.52881$].

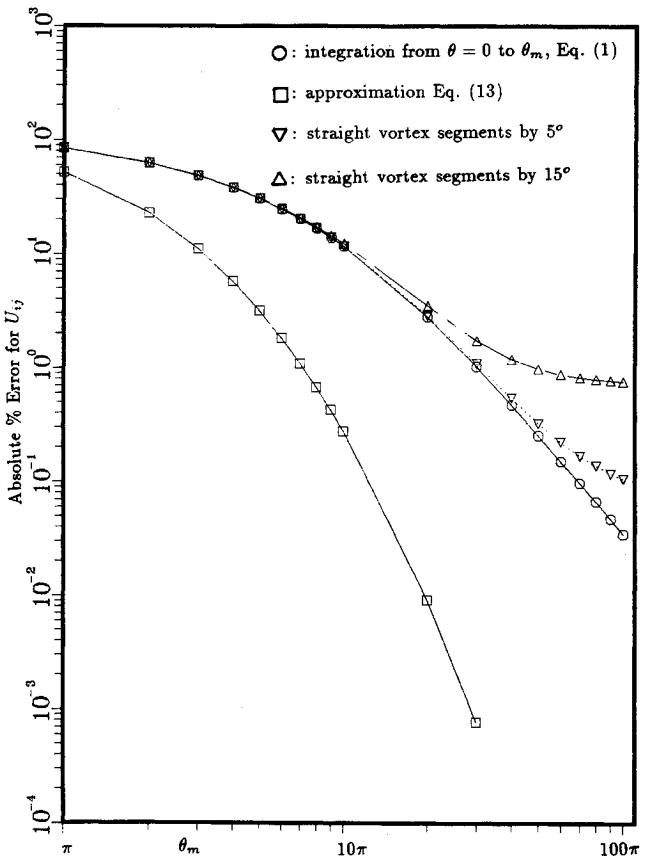

Fig. 14 Comparison of the influence coefficient U_{ij} with wake contraction as a function of the integration distance, θ_m, from Eqs. (1) and (13) [$b=2$; $k_1=0.125$; $k_2=0.0424$; $A=0.78$; $\lambda=0.1936$; $(x_i, y_i, z_i)/R=(0.95, 0, 0)$; exact value$=-15.5113$].

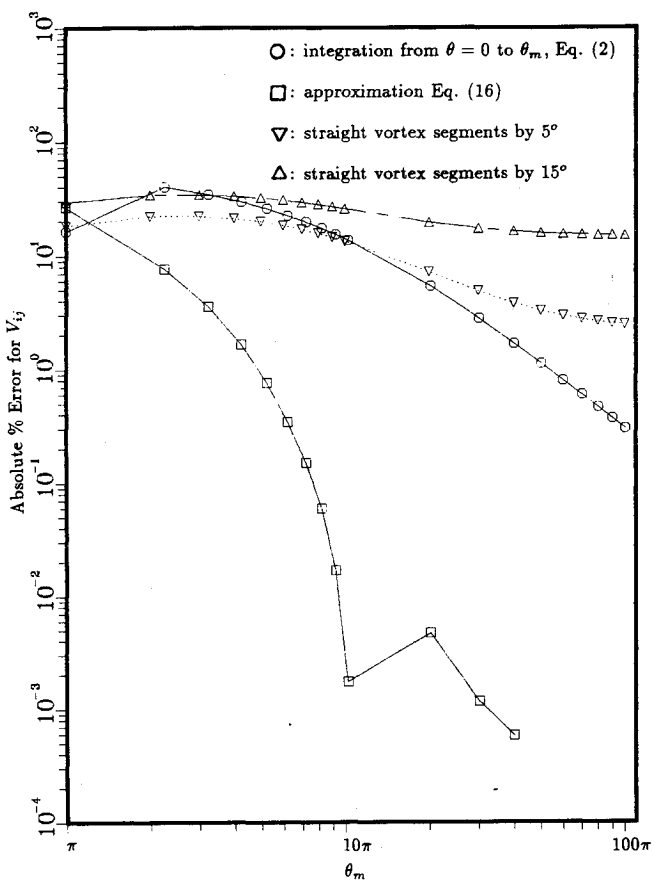

Fig. 15 Comparison of the influence coefficient V_{ij} with wake contraction as a function of the integration distance, θ_m, from Eqs. (2) and (16) [$b=2$; $k_1=0.125$; $k_2=0.0424$; $A=0.78$; $\lambda=0.1936$; $(x_i, y_i, z_i)/R=(0.95, 0, 0)$; exact value$=-1.70655$].

creases, the quadrature error (which is accumulated) *increases*, whereas the truncation error *decreases*. Thus, there comes a point for which the errors cancel (zero error asymptotes on Fig. 13). Beyond this, however, the quadrature error dominates; and 5-deg segments become better than 15-deg segments, although neither gives very good results. In contrast, the computation from the method in this paper shows good convergence throughout the range of θ_m. Figure 13 casts doubt as to whether or not even 5-deg segments ever converge.

Figures 14 and 15 show the corresponding plots for U_{ij} and V_{ij}. Here, the quadrature error does not cancel the truncation error (they are of the same sign), and 5-deg segments are more accurate than 15-deg segments. For U_{ij}, 5-deg segments seem to converge, but for V_{ij}, even 5 deg segments never give less than 2% error. Results from the approximate method give greater accuracy with less computer time than is required for discrete-vortex methods.

Conclusions

1) A general method is offered in which the trailing portion of the integral for all three induced velocity components can be found in closed form at any point in the flowfield even with wake contractions.

2) The use of this closed-form correction greatly improves convergence such that only 5 to 30% of the normal computing time is required.

3) An upper limit of 15 rotor revolutions is sufficient for 10^{-4} accuracy, and 3-5 revolutions give 1% error accuracy.

4) The quadrature error in vortex-segment methods grows with the number of revolutions and can dominate the error. This error is negligible in the present method.

5) More work needs to be done to see if this approach is beneficial in forward flight.

Acknowledgments

This work was sponsored by the United States Army Research Office, Grant Nos. DAAG-29-83-K-0133 and DAAG-29-85-K-0228. The view, opinions, and/or findings contained in this report are those of the authors and should not be construed as an official Department of the Army position, policy, or decision, unless so designated by other documentation.

References

[1]Lan, C., "A Quasi-Vortex-Lattice Method in Thin Wing Theory," *Journal of Aircraft*, Vol. 11, Sept. 1974, pp. 518–527.

[2]Margason, R. J. and Laman, J. E., "Vortex-Lattice Fortran Program for Estimating Subsonic Aerodynamic Characteristics of Complex Planforms," NASA TN D-6142, 1971.

[3]Belotserkouskii, *The Theory of Thin Wings in Subsonic Flow*, Plenum Press, New York, 1967.

[4]Chang, L. K., *The Theoretical Performance of High Efficiency Propellers*, Ph.D. Thesis, Purdue Univ., Lafayette, IN, 1980.

[5]Baskin, V. E., et al., "Theory of the Lifting Airscrew," NASA TTF-823, 1976.

[6]Summa, J. M. and Clark, D. R., "A Lifting-Surface Method for Hover/Climb Airload," Presented at 35th Annual National Forum of American Helicopter Society, Washington, DC, May 1979.

[7]Hess, J. L. and Valarezo, W. O., "Calculations of Steady Flow About Propellers by Means of a Surface Panel Method," presented at AIAA 23rd Aerospace Sciences Meeting, Reno, NV, Jan. 1985.

[8]Hough, G. R. and ordway, D. E., "The Generalized Actuator Disk," THERM Advanced Research Rept. TAR-TR6401, Jan. 1964.

[9]Rand, O. and Rosen, A., "Efficient Method for Calculating the Axial Velocities Induced Along Rotating Blades by Trailing Helical Vorticity," *Journal of Aircraft*, Vol. 21, June 1984, pp. 433–435.

[10]Rosen, A. and Graber, A., "Free Wake Model of Hovering Rotors Having Straight or Curved Blades," International Conference on Rotorcraft Basic Research, Research Triangle Park, NC, Feb. 1985.

[11]Graber, A. and Rosen, A., "Velocities Induced by Semi-Infinite Helical Vortex Filaments," *Journal of Aircraft*, Vol. 24, May 1987, pp. 289–290.

[12]Kocurek, J. D. and Tangler, J. L., "A Prescribed Wake Lifting Surface Over Performance Analysis," presented at 32nd Annual National Forum of American Helicopter Society, Washington, DC, May 1978.

[13]Landgrebe, A. J., "The Wake Geometry of a Hovering Helicopter Rotor and Its Influence on Rotor Performance," *Journal of the American Helicopter Society*, Vol. 16, Oct. 1972, pp. 1–15.

[14]Tung, C., et al., "The Structure of Trailing Vortices Generated by Model Rotor Blades," *Vertica*, Vol. 7, 1983, pp. 33–43.

[15]Norman, T. R. and Light, J. S., "Rotor Tip Geometry Measurements Using the Wide-Field Shadowgraph Technique," *Journal of the American Helicopter Society*, Vol. 32, April 1987, pp. 40–50.

Make Nominations for an AIAA Award

THE following awards will be presented during the 25th Joint Propulsion Conference, July 10–12, 1989, in Monterey, California. If you wish to submit a nomination, please contact Roberta Shapiro, Director, Honors and Awards, AIAA, 370 L'Enfant Promenade SW, Washington, D.C. 20024, (202) 646-7534. The deadline for submission of nominations in January 5, 1989.

Ground Testing Award

"For outstanding achievement in the development or effective utilization of technology, procedures, facilities, or modeling techniques for flight simulation, space simulation, propulsion testing, aerodynamic testing, or other ground testing associated with aeronautics and astronautics."

Air Breathing Propulsion Award

"For meritorious accomplishments in the science or art of air breathing propulsion, including turbo-machinery or any other technical approach dependent upon atmospheric air to develop thrust or other aerodynamic forces for propulsion or other purposes for aircraft or other vehicles in the atmosphere or on land or sea."

Wyld Propulsion Award

"For outstanding achievement in the development or application of rocket propulsion systems."